First-Principles Study of S Doping at the Rutile TiO_2 (110) Surface

Run Long[1], Niall J. English[*1],Ying Dai[2]

[1]The SEC Strategic Research Cluster and the Centre for Synthesis and Chemical Biology, School of Chemical and Bioprocess Engineering, Conway Institute of Biomolecular and Biomedical Research, University College Dublin, Belfield, Dublin 4, Ireland.

[2]School of Physics, Shandong University, Jinan, P. R. China 250100

Abstract: The structural, energetic and electronic properties of various S doping configurations by substitution and adsorption at the rutile TiO_2 (110) surface have been investigated by first-principles density functional theory (DFT) calculations. The stability of these configurations has been compared on the basis of the calculated formation and adsorption energies. Our results indicate that S dopants replace surface O atoms or bind to Ti atoms preferentially. Moreover, implantation of S dopants into the rutile lattice favored the formation of oxygen vacancies, which promotes further S incorporation. Doping of single S atoms into Ti sites (S-cation doping) led to relatively small reductions of the photon transition energy, while S-substitution of O atoms (S-anion doping) and adsorption on the surface (S-cation/anion doping) resulted in significant red-shifts of the optical absorption edge. Our results suggest that the interplay between S impurities and oxygen vacancies does not enhance visible light absorption in an obvious way, and helps to rationalise recent experimental

* Corresponding author: Email: niall.english@ucd.ie, Tel. +353-1-716 1646, Fax: +353-1-716 1177

studies.

Keywords: rutile TiO_2 (110) surface, S doping, electronic structure

Introduction

Titania has been used widely as a promising photocatalyst for water splitting and hydrogen production due to its high photocatalytic activity, resistance to photocorrosion, photostability, low cost and non-toxicity [1, 2]. Unfortunately, optical absorption of TiO_2 is limited to the ultraviolet region due to its large band gap (around 3.05 eV for rutile and 3.25 eV for anatase); the corresponding frequency ranges accounts for only about ~5% of solar irradiation. In the last decade or so, anion-doping of TiO_2 with non-metal elements, such as nitrogen [3-5] and carbon [6, 7], has attracted extensive scrutiny in an effort to narrow the band gap of TiO_2 and to shift the optical absorption edge towards the primary visible-light region.

Recently, many experiments have reported that S-doped TiO_2 can lead to significant redshifts of the optical absorption edge. In these studies, S-doping has been in either anion- or cation-doping modes [8-**11**]. Umebayashi et al. suggested that S was doped as an anion, and replaced the lattice O in TiO_2 [8]; this anion-doping shifted the absorption spectrum of TiO_2 to a lower energy, and it was observed that the absorption edge led to greater visible light activity. On the other hand, Ohno et al. have reported that S^{4+} were incorported as cations and replaced Ti^{4+} in S-doped TiO_2 [9, 10], and showed increased photocatalytic activity under visible light and stronger visible light absorption than N, C, and S anion-doped TiO_2. Yu et al. [11] synthesised S^{6+}-doped TiO_2 which exhibited a strong visible light-induced antibacterial effect. They reported that band gap-narrowing in this type of S-doped TiO_2 should be similar to conventional transition metal doping in titania. In terms of theoretical studies, band

gap-narrowing arising from S anion-doping in both anatase and rutile has been reported [8, 12]. Tian and Liu have suggested that the S 3p impurity above the valence band may be responsible for the redshift of the optical absorption edge in S anion-doped TiO_2 [13]. However, to our knowledge, all of the reported theoretical studies of S-doping in titania are focused on the bulk material.

Since many photo-reactivity properties of materials are influenced to a large extent by surface processes, analysis of doping characteristics at surfaces is of significant relevance. It has been shown that surface defects play an important role in the chemistry of TiO_2 [15, 16]. Therefore, the surface characteristics of a photocatalyst should be related closely with photocatalytic performances. In surface science, the rutile TiO_2 (110) surface has become probably the most studied oxide surface, and it is used to model TiO_2 catalytic properties under ultrahigh vacuum conditions [17, 18].

To obtain a comprehensive understanding of S-doped rutile TiO_2 (110) surfaces, we have performed DFT calculations to investigate the effects of S doping on electronic structure. We have considered various substitutional S anion- and cation-doping configurations at the surface and in subsurface layers, as well as the interplay between S dopants and bridging O vacancies. We have compared the stability of these different S-doping configurations according to their formation and adsorption energies. In addition, we have investigated the influence of single S-doping and the interaction between S dopants and oxygen vacancies on the electronic properties of doped TiO_2. Our theoretical analysis provides a possible explanation for the modification of band gaps reported by different experiments [8-11].

Computational Details

All of the spin-polarized DFT calculations were performed using projector augmented wave (PAW) pseudopotentials, as implemented in the Vienna *ab initio* Simulation Package (VASP) [19, 20]. The Perdew and Wang parameterisation [21] of generalized gradient approximation [22] was adopted for the exchange-correlation potential. The electron wave function was expanded in plane waves up to a cutoff energy of 400 eV, and a Monkhorst–Pack *k*-point mesh [23] of 2 × 2 × 1 was used for geometry optimisation and 4 × 4 × 1 for electronic property calculations. Both cell and atomic relaxations were carried out until the residual forces were below 0.01 eV/Å. The optimised lattice parameters of bulk rutile were found to be a = 4.608 Å and c = 2.956 Å, which agrees well with experimental values and other theoretical calculated results [24, 25]. For the electronic structure calculations, we used the GGA + U method introduced by Dudarev et al. [26]. The coupling parameter, U, was taken as 3.6 eV from previous work reported by Enevoldsen et al. [27]. Calzdo et al. [28] proved that the DFT+U approach could produce correct electronic properties of rutile (110) with surface oxygen vacancy using DFT geometry optimisation. Hence, in the present work, we used the DFT+U method to calculate electronic properties for both oxidized and reduced rutile (110) surfaces employed with DFT geometry optimisation.

The S-doped/adsorbed rutile TiO_2 (110) surface was modeled with a periodically repeated slab containing a 120-atom (2 × 2) reconstructed supercell consisting of five

TiO_2 layers (cf. Figure 1 (a)); this corresponded to a supercell depth of 30.53 Å. Each layer of TiO_2 was composed of three atomic sub-layers with a central plane containing Ti and O and two planes of bridging oxygen atoms above and below the central plane. The thickness of the vacuum layer above the slab was 15 Å, corresponding to a width of about 5 tri-layers. The atoms in the bottom layer were fixed to their optimised bulk positions in order to simulate the presence of the bulk underneath. This configuration has been shown to minimise well-known energy oscillations as a function of the number of layers (even-odd) [29].

Substitutional S-doping was modelled by replacing one O atom **or one Ti atom** per supercell with one S atom whereas adsorption of an S dopant was simulated by adding one S atom on the rutile TiO_2 (110) surface. The properties of a surface O vacancy were investigated by removal of one bridging O atom (O_v) on the surface, in the presence of either substitutional or adsorptive S species. To compare the relative stability of the S-doped surfaces, the formation energies E_f of the O-substituted systems were calculated according to formulae (1) and (2):

$$E_f = E(S-doped) - E(pure) - \mu_S + \mu_O \quad (1)$$

$$E_f = E(S-doped) - E(pure) - \mu_S + \mu_{Ti} \quad (2)$$

The following formula was used to calculate the S adsorption energy, E_{ad}:

$$E_{ad} = E(S-doped) - E(pure) - \mu_S \quad (3)$$

where $E(S-doped)$ is the total energy of the supercell containing the S impurity.

$E(pure)$ is the total energy either with or without the bridging surface O vacancy, as appropriate. μ_S, μ_O and μ_{Ti} denote the chemical potentials of the S, O, and Ti atoms, respectively. It should be noted that the formation energy depends on growth conditions, which may be either O- or Ti-rich [30]. μ_O and μ_{Ti} obey the relationship $\mu_{Ti} + \mu_O = \mu(TiO_2)$. Under Ti-rich growth conditions, μ_{Ti} is assumed to be the energy of one atom in bulk Ti (i.e. $\mu_{Ti} = \mu_{Ti}^{metal}$), and μ_O was calculated by the above formula. Under O-rich conditions, μ_O was calculated from an O_2 molecule (i.e. $\mu_O = \mu(O_2)/2$) and the chemical potential of Ti is found from the above formula. The chemical potential μ_S is calculated from **a** SO_2 molecule (i.e. $\mu_S = \mu(so_2) - \mu(o_2)$).

Results and Discussion

1. S implantation in stoichiometric rutile (110) surfaces

In this section, our main concern is to establish whether substitution in the surface is favoured with respect to substitution in a sub-layer. We consider two kinds of S doping, anion- and cation-doping, with various possible non-equivalent surface and sub-surface substitutional S dopant configurations. We limited substitution to the first two layers in the slab. Accordingly, there are five non-equivalent substitutions of S to O, namely, bridging (O_b), sub-bridging (O_{sb}), sub-bridging-2 (O_{sb2}), surface (O_s) and subsurface (O_{ss}) configurations. These are shown in Figure 1 (a). Conversely, there are two types of Ti atom on the rutile TiO_2 (110) surface. One is the six-fold coordinated Ti between the two bridging O atoms and the other is a five-fold

coordinated Ti in the sub-surface. Thus, we consider four possible substitutional configurations, namely, Ti_{5c}, Ti_{6c}, Ti_{s6c}, and Ti_{s6c2}.

1A. Substitutional S-doping in stoichiometric rutile (110) surfaces

The formation energies of the different substitutionally-doped systems are summarised in Table 1. The results indicate that sites can be ordered according to how thermodynamically favourable the substitution state, **however, it should be noted that the results from standard DFT only represent 0 K stability**. For S-anion doped systems, $O_b > O_s > O_{sb} > O_{sb2} > O_{ss}$, while the corresponding results for S-cation doping are $Ti_{6c} > Ti_{s6c2} > Ti_{5c} > Ti_{s6c}$. This indicates that S dopants occupy surface bridging oxygen O_b sites preferentially in both O- and Ti-rich growth conditions. This is different from N-doped rutile (101) surfaces [31], where preferential occupation takes place at the O_{sb} site. **The possible reason is that the small N ion can easily incorporate into subsurface O site while the larger P prefers to occupy the surface O position. At the same time, a possible reason for N preferring to locate at the O_{sb} site rather than the O_b site is that two stronger O-Ti bonds at the surface (O1-TiA(B)) incline N to occupy the subsurface O_{sb} site than three relatively weak O-Ti bonds (O6-TiA(B)(F)) in the subsurface (see Tables 1 and 2).** The results show also that Ti-rich growth conditions are energetically favourable for S-anion doping while S-cation doping is preferential under O-rich conditions. This conclusion is in agreement with the experimental findings of Umebayashi et al., in which S acts as an anion in TiO_2 [8]. Conversely, in

the case of S-cation doping, six-fold coordinated surface sites (Ti_{6c}) constitute the most stable position in stoichiometric rutile TiO_2 (110) surfaces under both O- and Ti-rich growth conditions. Further, the formation energy is smaller under O-rich growth conditions **than that of Ti-rich growth conditions, which suggests that the synthesis of S-cation-doped titania should take O-rich growth conditions preferentially.** This is supported by the experimental findings of Yu et al. [11] and Ohno et al. [9, 10]. Therefore, our theoretical calculations indicate that the form of the S ion in S-doped TiO_2 (i.e. anion or cation) depends on the growth conditions. **Although experiments have not been in a position to yield the exact positions of substitutional S, theoretical investigations can handle this matter via selection of most possible defective configurations based on the calculated formation energies. This method has been used by different authors to deal with various doping systems [32-34] and to obtain reasonable results relative to experiments. In particular, the formation energies are 3.08 and 0.85 eV for O_b and Ti_{6c} under Ti-rich and O-rich growth conditions, respectively, which indicates that they are the most probable occurring defective configurations in experiments.** Given this, we shall only discuss the details of structural and electronic properties for the most stable cases of S-substitutional doping at O_b and Ti_{6c} sites at stoichiometric rutile (110) surfaces.

The optimised partial geometrical structures are shown in Figure 2. For the O_b-substituted case **(cf. Figure 2(a))**, the S atom forms two S-Ti bonds by trapping electrons from the adjacent two Ti atoms. The two S-Ti bond lengths were 2.300 Å,

which results in significant structural distortion in comparison to the relaxed Ti_A-O_1 bond length (1.848 Å), due to the larger atomic radius of the S atom vis-à-vis the O atom. For the Ti_{6c}–substituted case **(cf. Figure 2(b))**, the two optimal shortest S-O bonds were found to be 1.484 Å, slightly larger than the bond length in the SO_2 molecule (1.481 Å); this is some 0.364 Å shorter than the Ti_A-O_1 (1.848 Å) (see Figure 1(a) and Table 1).

1B. S adsorption on stoichiometric rutile (110) surfaces

For S adsorption on (110) surfaces, there are six non-equivalent sites, namely, Top-O_b, Top-O_s, Top-Ti_{5c}, Top-Ti_{6c}, Cave, and Hollow. These are shown in Figure 1(b). Table 2 (on the left panel) summarises the results for the adsorption energies at each different position on the stoichiometric surface. The corresponding thermodynamic stability of the systems are: Top-Ti_{6c} > Top-O_s > Top-O_b > Hollow > Cave > Top-Ti_{5c}. The Top-Ti_{6c} case is the most stable system with a value of 6.04 eV and the Top-Ti_{5c} is the least stable system with an adsorption energy of 7.96 eV. It is worth noting that this configuration has two S-O distances of 1.622 Å and an S-Ti bond length of 2.781Å **(cf. Figure 2(c))**. We shall discuss the electronic structures of Top-Ti_{6c}-adsorbed case on stoichiometric surfaces.

1C. Oxidation state of S dopant

To study the variation of the oxidation state of the S dopant, the total charge densities **on the (001) surface** for S-doping in the O_b, Ti_{6c} and **Top-Ti_{6c}** cases were

calculated, and are shown in Figures **3** (a)-(c) (top panel). Figure **3**(a) shows the contour plot of charge density near the surface for the O_b–substituted system, in which the S atom and adjacent Ti atoms form two S-Ti bonds, implying a negative oxidation state. For the Ti_{6c}-substituted case, Figure **3**(b) shows that the S atom forms six S-O bonds (shown only in one plane), indicating a positive oxidation state. For the Top-Ti_{6c}-adsorbed case, two S-O bonds are formed, along with a single S-Ti bond. The S-O bond was found to be stronger the S-Ti bond, implying that S exists as a cation. To confirm this, we calculated the Bader charge [**35**, **36**] of the S atom in the O_b, Ti_{6c}, and Top-Ti_{6c} cases, and found that the corresponding Bader charges on the S atom in O_b, Ti_{6c} and Top-Ti_{6c} sites are -1.17 |e| and 3.11 |e|, and 1.89 |e|, implying an anionic state for the S dopant in the O_b-substituted case, and a cationic state for the Ti_{6c}–substituted and Top-Ti_{6c}-adsorbed configurations. This analysis supports various experimental findings that S-doping doping can lead to either anionic or cationic states [8-11].

1D. Electronic structure of substitutional and adsorptive S-doping at stoichiometric surfaces

To investigate the effects of the substitutional and adsorptive S-doping motifs on electronic structures and photocatalytic activity, the density of states (DOS) and projected density of states (PDOS) of O_b, Ti_{6c} and Top-Ti_{6c} systems were calculated, and are shown in Figure **4**. For comparison, the DOS and PDOS of the pure rutile (110) surface are shown also. There are substantial differences in the electronic

structure between the three doping cases. For the O_b (S anion-doping) model (cf. Figures **4** (b) and (b')), the DOS shows that the impurity states lie above the valence band maximum (VBM) and are mixed with O 2p states, while the PDOS indicates that the impurity states are composed mainly of S 3p atomic orbitals. The transition energy for electron excitation from the valence band to the conduction band minimum (CBM) is reduced by about 0.23 eV vis-à-vis the pure state, corresponding to a red-shift of the optical absorption edge. Further, a large portion of S 3p states extend in energy into the band gap with a maximum of about 0.9 eV from the VBM of the (110) surface, leading the Fermi level, E_F, to locate above the localized states. Thus, the transition from these occupied S 3p states to the conduction band may also lead to a decrease in the photon excitation energy and result in a more obvious red-shift of the absorption edge. Recent experiments [**37**] have confirmed that a significant red-shift takes place from 400 nm to 560 nm in S-doped TiO_2, corresponding to a reduction of 0.89 eV in the transition energy.

For the Ti_{6c} (S cation-doped) system (cf. Figures **4** (c) and (c')), the VBM and CBM exhibit little change vis-à-vis the pure surface, and most of the S 3p impurity states are located in the lower energy region. The hybrid S 3s-S 3p states lie in the band gap, in which the interval between the gap states and the VBM is around 1.24 eV, leading to reduction of approximately 0.86 eV in the band gap. Consequently, electrons occupying the gap states will require less energy to transfer to the conduction band, leading to a significant red-shift of visible light region. This accounts well for the large red-shift from 410 nm to 550 nm (corresponding to a

reduction in absorption energy by around 0.77 eV) reported in experiments [9] with S cation doping.

For S adsorption on the Top-Ti_{6c} site (S cation-doping), the DOS (cf. Figure **4**(d)) shows that the localized states lie in the band gap and the Fermi level E_F was pinned to the tail of the gap states. The PDOS (cf. Figure **4**(d')) shows that the gap states are composed mostly of S 3p states. This suggests that electron excitation can occur from the VBM for occupied S 3p states to unoccupied S 3p states and then to the CBM. The process corresponds to a significant reduction in the band gap, and extends to longer wavelengths. The largest reduction in transition energy is as large as 1.48 eV. These results suggest that S cation-doping will lead to better photocatalytic activity and larger absorption wavelengths relative to S anion-doping. Our calculated results provide an explanation for the observed red-shifts and trends in photocatalytic activity of S-doped TiO_2 in various different experiments [8-11].

2. S implantation in non-stoichiometric rutile TiO_2 (110) surfaces

The reactivity of the TiO_2 (110) surface is highly influenced by oxygen vacancies, the most frequent of which is that corresponding to surface bridging oxygen atoms. In this section, our main aim is to investigate whether the bridging oxygen vacancy (O_V) promotes or hinders S substitution and adsorption. Therefore, we calculated the formation and adsorption energies for S anion- and cation-doping at the non-stoichiometric rutile TiO_2 (110) surface. In addition, we analysed the structural and electronic properties based on these energy results.

2A. Substitutional and adsorptive S-doping at non-stoichiometric rutile TiO_2 (110) surfaces

Non-stoichiometric surfaces arise due to O-poor conditions, due to deficient oxygen. Therefore, we only calculated the formation and adsorption energies under O-poor conditions. Table 1 (right panel) and Table 2 (right panel) summarise the calculated formation and adsorption energies, respectively. The stability of substitutionally-doped systems was found to be in the following order: (1) for S anion-doping, $O_b > O_s > O_{sb} > O_{sb2} > O_{ss}$; (2) for S cation-doping, $Ti_{6c} > Ti_{5c} > Ti_{s6c2} > Ti_{s6c}$. This indicates that the most stable configurations are still the O_b and Ti_{6c} models for S anion- and cation-doping, respectively. The formation energies are slightly smaller than those of the stoichiometric surface, indicating that incorporation of S promotes the formation of oxygen vacancies. Conversely, the formation of oxygen vacancies favours the implantation of S. For S adsorptive-doped systems, the stability was in the order: Top-Ti_{5c} > Cave > Top-O_s > Hollow > Top-Ti_{6c} > Top-O_b. The Top-Ti_{5c}-adsorbed system became the most stable configuration rather than the Top-Ti_{6c} -adsorbed case, with an adsorption energy of 5.10 eV. This suggests that S may be adsorbed easily on the rutile (110) surface with oxygen vacancies. Therefore, we shall study the structural and electronic properties of O_b- and Ti_{6c}-substituted and Top-Ti_{5c}-adsorbed systems in detail.

The optimised partial geometrical structures are shown in Figure 2. For the O_b–substituted system **(cf. Figure 2(d))**, there were two S-Ti bonds, both of which

were 2.305 Å in length, which increased slightly by about 0.005 Å relative to their equivalents in the stoichiometric surface (2.300 Å), due to local geometry distortion from removal of the bridging oxygen atom. For the Ti_{6c}-substituted case **(cf. Figure 2(e))**, the optimised bond lengths of the two S-O bonds were 1.486 Å, a small change of about 0.002 Å in comparison to the S-O bond lengths (1.484 Å) for the Ti_{6c}-substituted case at the stoichiometric surface. For the Top-Ti_{5c}–adsorbed system **(cf. Figure 2(f))**, the optimised S-Ti bond length was 2.106 Å. The Bader charges on the S impurity atom were found to be -1.25 |e|, 3.35 |e|, and -1.04 |e|, for the O_b–substituted, Ti_{6c}-substituted and Top-Ti_{5c}–adsorbed systems, respectively. This indicates that substitution of S for O_b and adsorption of S at the Ti_{5c} site correspond to anion-doping, and substitution of S for Ti_{6c} leads to cation-doping. To examine further changes in the S oxidation state in the three systems, the charge density maps **on the (001) surface** have been presented in Figures **3**(d)-(f) (bottom panel). Similar to the analysis in section 1C, Figures **3**(d), (e), (f) indicate that the S dopant exists in anionic, cationic, and anionic states in the O_b–substituted, Ti_{6c}-substituted and Top-Ti_{5c}–adsorbed systems, respectively. This helps to rationalize the findings of various experiments which find that S dopants may be either anionic or cationic, depending on conditions [8-11].

2B. Electronic structure of substitutional and adsorptive S-doping on non-stoichiometric rutile TiO_2 (110) surfaces

To investigate the interplay between substitutional/adsorptive S dopant and the

bridging oxygen vacancy on electronic structures and photocatalytic activity, the density of states (DOS) and projected density of states (PDOS) of the O_b, Ti_{6c} and Top-Ti_{5c} systems were calculated, and are shown in Figure **5**. For comparison, the DOS and PDOS of perfect rutile TiO_2 (110) surface are also shown. **However, before investigating the interplay of the bridging O vacancy (O_V) with the S impurity, the electronic properties of O_V need to be considered. The removal of a neutral surface bridging O atom causes the adjacent Ti atoms to change from the Ti^{4+} to the Ti^{3+} state, as reported experimentally [38]. The DOS and PDOS (cf. Figures 5(b) and (b')) show that the localized Ti 3d states lie below the CBM. This conclusion is consistent with previous theoretical and experimental studies [38, 39].** Figure **5** shows significant differences in the electronic structure between the three doping cases. For the O_b–substituted case (S anion-doping) (cf. Figures **5 (c)** and **(c')**), the locations of the S 3p impurity states show nearly no change with respect to O_b-substitution in the stoichiometric surface (cf. Figures **4** (b) and (b')), but the Fermi level, E_F, is pinned below the conduction band. At the same time, some Ti^{3+} impurity levels lie close to the CBM. This leads to a larger electron transition energy from the S 3p states above the VBM to states above E_F compared to the undoped non-stoichiomeric surface. However, the transition energy from the S 3p gap states to the states above E_F is reduced by about 0.95 eV, which is quite close to the corresponding 1.08 eV for a single S atom locating at the O_b site. This may also be responsible for a significant red-shift from 400 nm to 560 nm in S anion-doped TiO_2 observed experimentally [32]. For the Ti_{6c}–substituted (S cation-doped) case (cf.

Figures **5(d)** and **(d')**), there are no obvious differences except some Ti^{3+} impurity states appeared in the band gap relative to the corresponding system for the non-stoichiometric surface (see Figures **4(c)** and **(c')**): for the non-stoichiometic case, the S 3s-3p hybridised states lie near the VBM, leading the Fermi level E_F to locate below the conduction band. This leads to a reduction of 0.48 eV in the electron transfer energy from the S 3p states to the states above the E_F with respect to the undoped surface (0.66 eV for the non-stoichiometric case). It results also in a significant red-shift of the optical absorption edge. For the Top-Ti_{5c}–adsorbed (S anion-doped) system (Figures **5(e)** and **(e')**), the DOS shows that the two impurity states lie in the band gap while the Fermi level E_F locates between them, indicating that one is fully occupied and the other unoccupied. The distance between the two states was 0.90 eV, indicating that electron transition energy is reduced by about 1.2 eV compared to the perfect surface. Therefore, this analysis shows that the interaction between the S impurity and the oxygen vacancy does not lead to greater visible light absorption region in an obvious fashion.

Conclusions

We have presented comprehensive calculations of S doping at the rutile TiO_2 (110) surface using DFT methods. The formation energies indicate replacement of the bridging oxygen on the surface by S atoms is the most energetically favoured doping model. Further, under Ti-rich growth conditions, incorporation of S into O sites is energetically preferential for both stoichiometric and non-stoichiometric surfaces.

When S is adsorbed on rutile (110) surfaces, the most stable configuration is S at the **Top-Ti_{6c}** site on the stoichiometric surface, while replacement of the five-coordinated Ti atom by S atom is favoured on the non-stoichiometric surface. The calculated Bader charges and the charge density have shown that S dopants may exist as either anions or cations. The calculated DOS shows that single S anion-doping will induce a slight narrowing of the band gap and introduce some S 3p states lying in the band gap of TiO_2. This conclusion helps to rationalize experimental observations of S anion-doping leading to either band-to-band transitions or addition of gap states to band transition, corresponding respectively to slight [8] and large [31] band gap reductions. However, S cation-doping can lead to significant reductions of photon transition energies due to S 3p gap states, confirmed by experimental observations of a 0.77 eV reduction in the band gap [9]. The interplay between the S dopant and the O vacancy should modify significantly the position of the Fermi level, but does not lead to an obvious enhancement in visible light absorption. Our conclusions provide a reasonable explanation for experimental observations of lower photon absorption energies and higher photocatalytic activity under visible light irradiation with S anion- and cation-doped TiO_2.

Acknowledgements

This work was supported by the Irish Research Council for Science, Engineering and Technology (IRCSET). The authors thank the Irish Centre for High End Computing and Science Foundation Ireland for the provision of computational resources. Prof.

Ying Dai thanks for the National Basic Research Program of China (973 program, Grant No. 2007CB613302), National Natural Science Foundation of China under Grant No. 10774091, Natural Science Foundation of Shandong Province under Grant No. Y2007A18, and the Specialized Research Fund for the Doctoral Program of Higher Education 20060422023.

References

(1) Fujishim, A.; Honda, K. *Nature* **1972**, *238*, 37.

(2) Diebold, U. *Surf. Sci. Rep.* **2003**, *48*, 53.

(3) Asahi, R.; Morikawa, T.; Ohwaki, T.; Aoki, K.; Taga, Y. *Science* **2001**, *293*, 1457.

(4) Sato, S. *Chem. Phys. Lett.* **1986**, *123*, 126.

(5) Batzill, M.; Morales, E. H.; Diebold, U. *Phys. Rev. Lett.* **2006**, *96*, 026103.

(6) Tashikawa, T.; Tojo, S.; Kawai, K.; Endo, M.; Fujitsuka, M.; Ohno, T.; Nishijima, K.; Miyamoto, Z.; Majima, T. *J. Phys. Chem. B* **2004**, *108*, 19299.

(7) Barborini, E.; Conti, M A.; Kholmanov, I. N.; Miseri, P.; Podestå, A.; Milani, P.; Cepek, C.; Sakho, O.; Macovez, R.; Sancrotti, M. *Adv. Mater.* **2005**, *17*, 1842.

(8) Umebayashi, T.; Yamaki, T.; Itoh, H.; Asai, *Appl. Phys. Lett.* **2002**, *81*, 454.

(9) Ohno, T.; Mitsui, T.; Matsumura, M. *Chem. Lett.* **2003**, *32*, 364.

(10) Ohno,T.; Akiyoshi, M.; Umebayashi, T.; Asai, K.; Mitsui, T.; Matsumura, M. *Appl. Catal., A* **2004**, *265*, 115.

(11) Yu, J. C.; Ho, W.; Yu, J.; Yip, H.; Wong, P. K.; Zhao, J. *Environ. Sci. Technol.* **2005**, *39*, 1175.

(12) Yamamoto, T.; Yamashita, F.; Tanaka, I.; Matsubara, E.; Muramatsu, A. *Mater. Trans.* **2004**, *45*, 1987.

(13) Tian, F.; Liu, C. *J. Phys. Chem. B* **2006**, *110*, 17866.

(14) Yang, K. S.; Dai, Y.; Huang, B. B. *J. Phys. Chem. C* **2007**, *111*, 18985.

(15) Henderson, M. A. *Surf. Sci.* **1996**, *355*, 1511.

(16) Henderson, M. A.; Epling, W. S.; Pede, C. H. F.; Perkins, C. J. *J. Phys. Chem. B* **2003**, *107*, 534.

(17) Henderson, M. A. *Surf. Sci. Rep.* **2002**, *46*, 5.

(18) Bondarchuk, O.; Kim, Y. K.; White, J. M.; Kim, J.; Kay, B. D.; Dohnalek, Z. *J. Phys. Chem. C* **2007**, *111*, 11059.

(19) Kresse G.; Furthműller, J. *Comput. Mater. Sci.* **1996**, *6*, 15.

(20) Kresse, G.; Furthműller, J. *Phys. Rev. B* **1996**, *54*, 11169.

(21) Perdew, J. P.; Burk, K.; Ernzerhof, M. *Phys. Rev. Lett.* **1996**, *77*, 3865.

(22) Perdew, J. P.; Wang, Y. *Phys. Rev. B* **1992**, *45*, 13244.

(23) Monkhorst, H. J.; Pack, J. D. *Phys. Rev. B* **1976**, *13*, 5188.

(24) Thompsom, S. J.; Lewis,S. P. *Phys. Rev. B* **2006**, *73*, 073403.

(25) Burdett, J. K.; Hughbanks, T.; Miller, G. J.; Richardson, J. W. Jr.; Smith, J. V. *J. Am. Chem. Soc.* **1987**, *109*, 3639.

(26) Dudarev, S. L.; Botton, G. A.; Savarsov, S. Y.; Humphreys, C. J.; and Sutton, A. P. *Phys. Rev. B* **1998,** *57,* 1505

(27) Enevoldsen, G. H.; Pinto, H. P.; Foster, A. S.; Jensen, M. C. R.; Hofer, W. A.; Hammer, B.; Lauritsen, J. V.; and Besenbacher, F. *Phys. Rev. Lett.* **2009**, *102*,

136103.

(28) Calzado, C. J.; Hernández, N. C.; and Sanz, J. F. *Phys. Rev. B* **2008**, *77*, 045118.

(29) Berdow, T.; Giordano, L.; Cinquini, F.; Pacchioni, G. *Phys. Rev. B* **2004**, *70*, 035419.

(30) Wall, C. G. V.; Neugebauer, J. *J. Appl. Phys.* **2004**, *95*, 3851.

(31) Graciani, J.; Alvarez, L. J.; Rodriguez, J. A.; Sanz, J. F. *J. Phys. Chem. C* **2008**, *112*, 2624.

(32) Long, R.; English, N. J. *J. Phys. Chem. C* 2009 *113*, 9423.

(33) Long, R.; English, N. J. *Appl. Phys. Lett.* 2009, *94*, 132102.

(34) Mi. L.; Xu, P.; Shen, H.; Wang, P. N. *Appl. Phys. Lett.* 2007, *90*, 171909.

(35) Davidson, E. R. *Methods in Computational Molecular Physics* edited by G.H.F. Diercksen, Reidel, Dordrecht, 1983

(36) Wilson, S. Vol. 113 *NATO Advanced Study Institute, Series C* (Plenum, New York, 1983), p. 95.

(37) Ho, W.; Yu, J. C.; Lee, S. *J. Solid. State Chem.* **2006**, *179*, 1171.

(38) Nambu, A.; Graciani, J.; Rodríguez, J. A.; Wu, Q.; Fujita, E.; Sanz, J. *J. Chem. Phys.* 2006, *125*, 094708

(39) **Morgan, B. J.; Waston, G. W. *Surf. Sci.* 2007, *601*, 5034.**

Table 1. Formation energies (in eV) for S doping in different positions at the rutile TiO_2 (110) surface.

	Formation energies (eV)	
Positions	Stoichiometric	Non-stoichiometric
	Ti-rich (O-rich)	Ti-rich
O_b	*3.08 (8.05)*	*2.76*
O_s	*3.37 (8.34)*	*3.09*
O_{sb}	*3.49 (8.46)*	*3.13*
O_{sb2}	*4.62 (9.59)*	*4.16*
O_{ss}	*5.15 (10.12)*	*4.99*
Ti_{5c}	*12.24 (2.31)*	*11.08*
Ti_{6c}	*10.78 (0.85)*	*10.41*
Ti_{s6c}	*12.39 (2.46)*	*12.08*
Ti_{s6c2}	*12.06 (2.13)*	*11.30*

Table 2. Adsorption energies (in eV) for S at different positions of rutile TiO_2 (110) surfaces. The corresponding labels can be found in Figure 1(b).

Positions	Adsorption energies (eV)	
	Stoichiometric	Non-stoichiometric
Cave	*7.90*	*5.84*
Hollow	*6.48*	*5.85*
Top-O_b	*6.32*	*6.16*
Top-O_s	*6.10*	*5.85*
Top-Ti_{5c}	*7.96*	*5.10*
Top-Ti_{6c}	*6.04*	*6.11*

Figure captions

Figure 1. Structure of rutile TiO_2 (110) surface. (a) Side view, (b) Top view. The non-stoichiometric surface corresponds to removal of one bridging oxygen atom (denoted by 1 in (a)). The large light and small dark spheres represent Ti and O atoms, respectively. The numbers and the block letters are used for identification purposes.

Figure 2. Optimised partial geometrical structures: (a) O_b, (b) Ti_{6c}, and (c) Top-Ti_{6c} at stoichiometric rutile TiO_2 (110) surfaces (top panel). (d) O_b, (e) Ti_{6c}, and (f) Top-Ti_{5c} on non-stoichiometric rutile TiO_2 (110) surfaces (bottom panel). The large light, small dark, and yellow spheres represent Ti, O, and S atoms, respectively.

Figure 3. Total electron density contours **on the (001) surface** in the vicinity of the S-dopant: (a) O_b, (b) Ti_{6c}, and (c) Top- Ti_{6c} at stoichiometric rutile TiO_2 (110) surfaces. (d) O_b, (e) Ti_{6c}, and (f) Top-Ti_{5c} on non-stoichiometric rutile TiO_2 (110) surfaces.

Figure 4. (A) Density of states (DOS) for S-doping at stoichiometric rutile TiO_2 (110) surfaces: (a) pure surface, (b) O_b system, (c) Ti_{6c} configuration, and (d) Top- Ti_{6c} model. (B) Corresponding projected density of states (PDOS) were shown in (a') - (d'). The top of the valence band of the pure rutile TiO_2 (110) surface has been taken as the reference level. The dashed lines represent the Fermi level E_F.

Figure 5. (A) DOS for S-doping at non-stoichiometric rutile TiO_2 (110) surfaces: (a) undoped surface, **(b) O_V model, (c)** O_b case, **(d)** Ti_{6c} system, and **(e)** Top-Ti_{5c} configuration. (B) Corresponding PDOS were shown in (a') - (e'). The top of valence

band of the pure surface has been adopted as the reference, while the dashed lines denote the Fermi level, E_F.

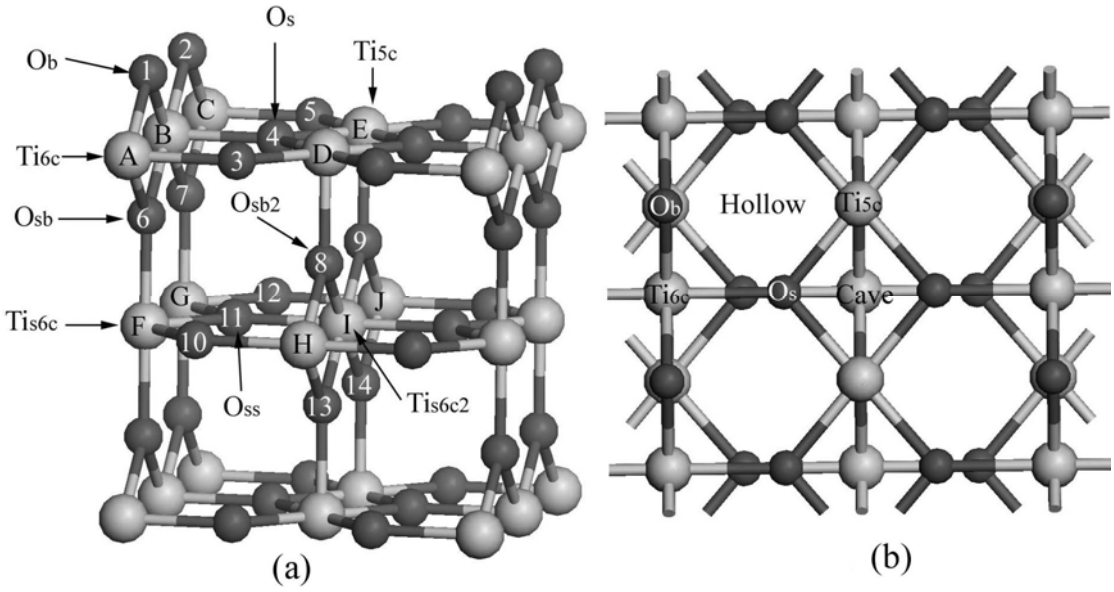

Figure 1

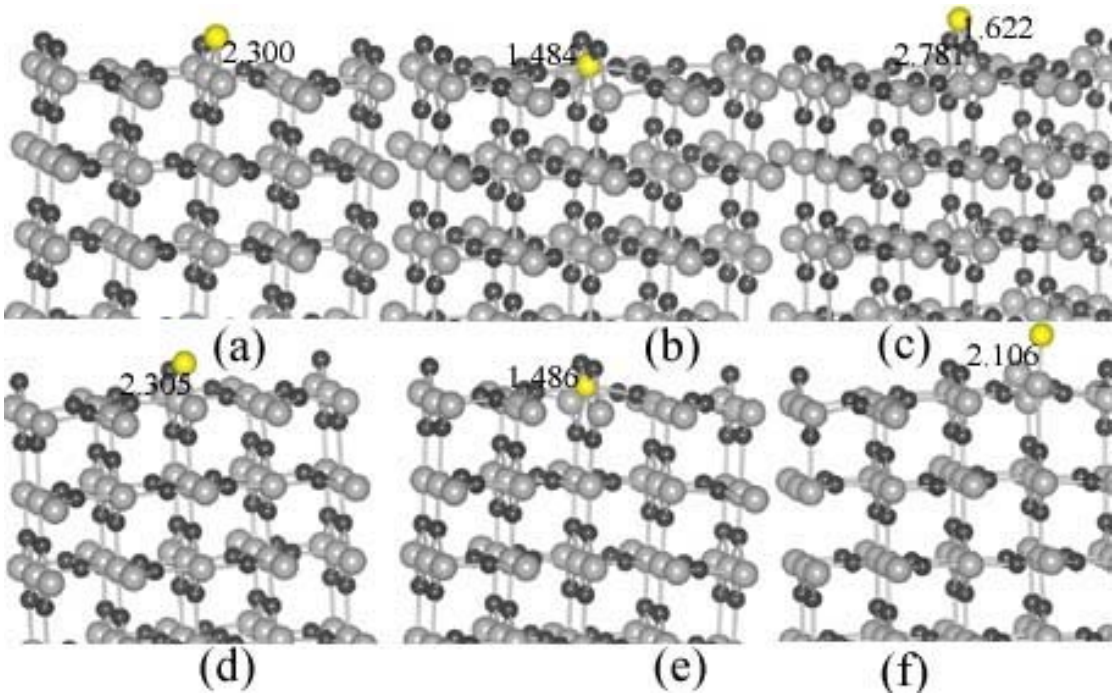

Figure 2

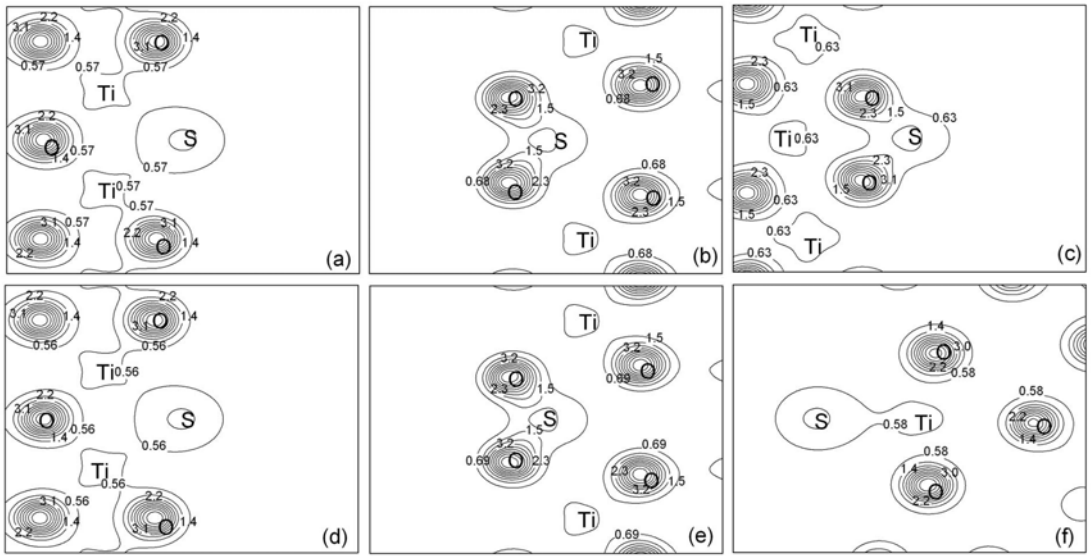

Figure 3

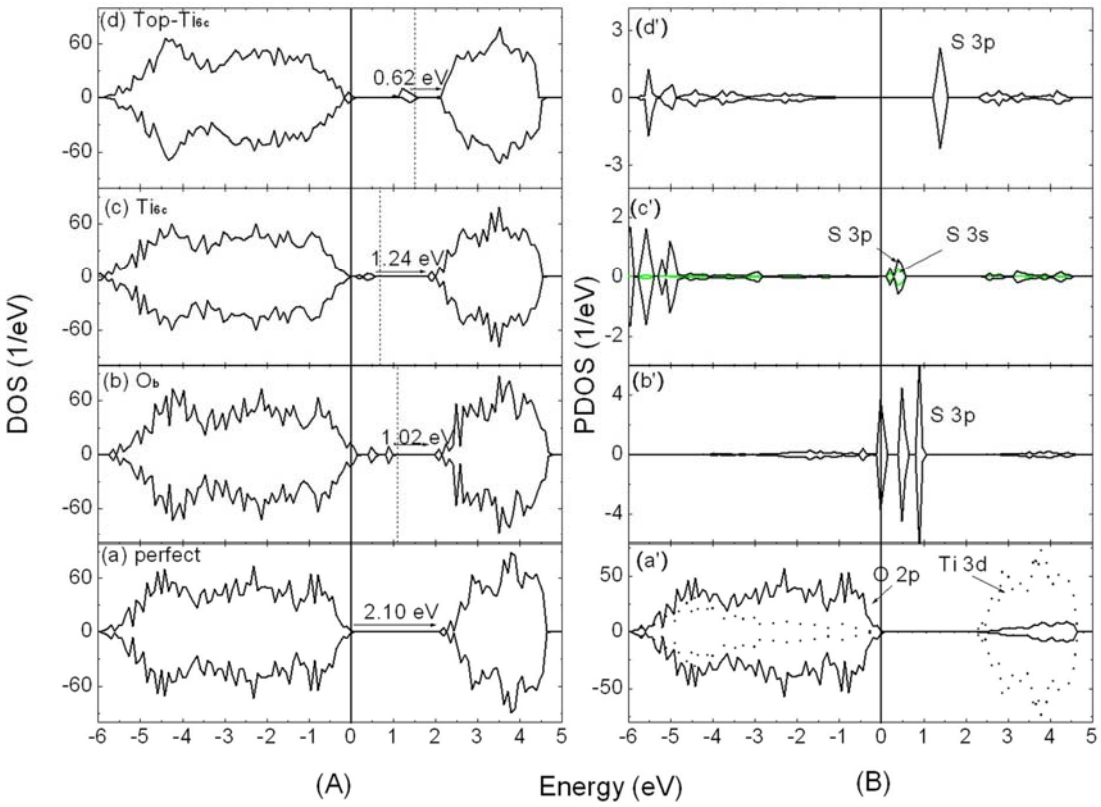
(d) Top-Ti6c
0.62 eV
(c) Ti6c
1.24 eV
(b) Ob
1.02 eV
(a) perfect
2.10 eV
DOS (1/eV)
(d')
S 3p
(c')
S 3p
S 3s
(b')
S 3p
(a')
O 2p
Ti 3d
PDOS (1/eV)
(A)
Energy (eV)
(B)

Figure 4

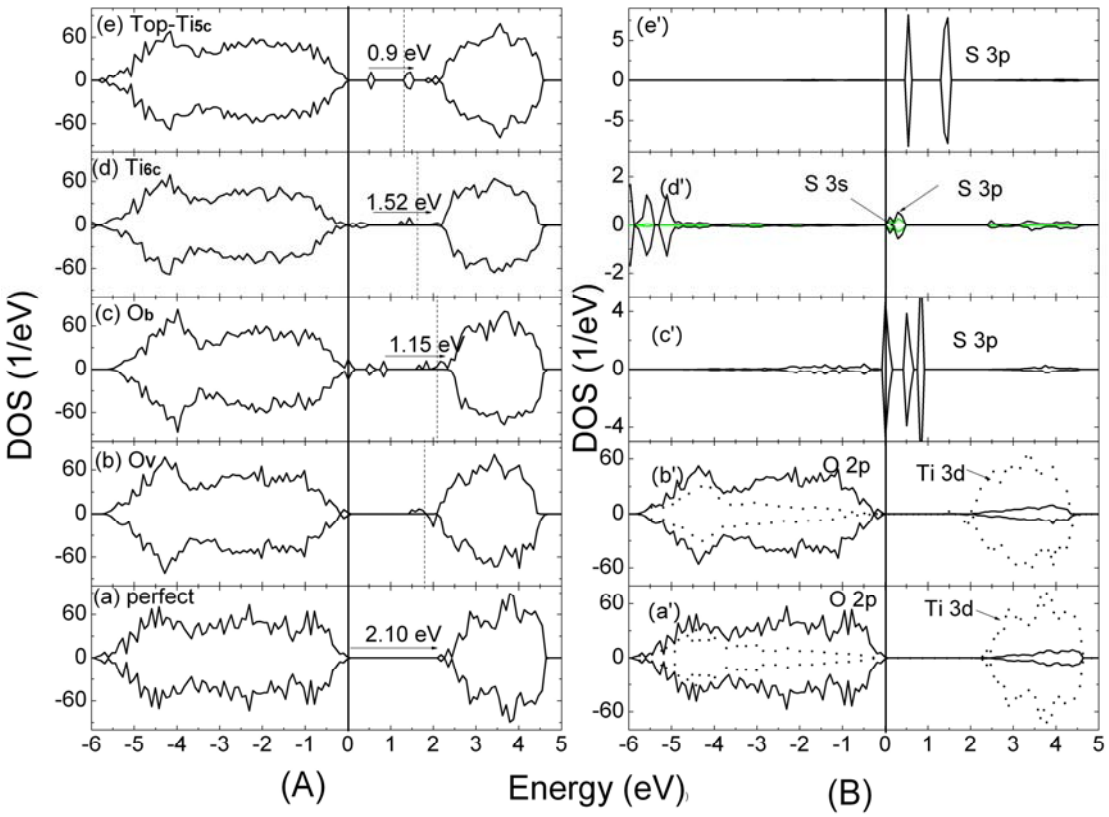
(e) Top-Ti5c
0.9 eV
(d) Ti6c
1.52 eV
(c) Ob
1.15 eV
(b) Ov
(a) perfect
2.10 eV
DOS (1/eV)
(A)
Energy (eV)
(e')
S 3p
(d')
S 3s
S 3p
(c')
S 3p
(b')
O 2p
Ti 3d
(a')
O 2p
Ti 3d
DOS (1/eV)
(B)

Figure 5